

Combinational Quorum Sensing Devices for Dynamic Control in Cross-feeding Cocultivation

Shengbo Wu^{1,2}, Yanting Xue¹, Shujuan Yang¹, Chengyang Xu¹, Chunjiang Liu^{1,2,4},
Xue Liu^{1,5,6}, Jiaheng Liu^{1,5,6}, Hongji Zhu^{1,5,6}, Guang-Rong Zhao^{1,4,5,6}, Aidong Yang^{3*},
Jianjun Qiao^{1,4,5,6*}

¹School of Chemical Engineering and Technology, Tianjin University, Tianjin, 300072, China

²State Key Laboratory of Chemical Engineering, Tianjin University, Tianjin 300072, China

³Department of Engineering Science, University of Oxford, Oxford OX1 3PJ, UK

⁴Collaborative Innovation Center of Chemical Science and Engineering (Tianjin), Tianjin, 300072, China

⁵Key Laboratory of Systems Bioengineering, Ministry of Education (Tianjin University), Tianjin, 300072, China

⁶Frontiers Science Center for Synthetic Biology (Ministry of Education), Tianjin University, Tianjin, 300072, China

*Correspondence and requests for materials should be addressed to

Aidong Yang (email: aidong.yang@eng.ox.ac.uk)

Jianjun Qiao (email: jianjunq@tju.edu.cn)

Abstract

Quorum sensing (QS) offers cell density dependent dynamic regulations in cell culture through devices such as synchronized lysis circuit (SLC) and metabolic toggle switch (MTS). However, there is still a lack of studies on cocultivation with a combination of different QS-based devices. Taking the production of isopropanol and salidroside as case studies, we have mathematically modeled a comprehensive set of QS-regulated cocultivation schemes and constructed experimental combinations of QS devices, respectively, to evaluate their feasibility and optimality for regulating growth competition and corporative production. Glucose split ratio is proposed for the analysis of competition between cell growth and targeted production. Results show that the combination of different QS devices across multiple members offers a new tool with the potential to effectively coordinate synthetic microbial consortia for achieving high product titer in cross-feeding cocultivation. It is also evident that the performance of such systems is significantly affected by dynamic characteristics of chosen QS devices, carbon source control and the operational settings. This study offers insights for future applications of combinational QS devices in synthetic microbial consortia.

Key words: Quorum Sensing; synchronized lysis circuit; metabolic toggle switches; microbial community; biofuels; glycosides; synthetic biology.

1. Introduction

The development of metabolic engineering has enabled the biosynthesis of a wide range of valuable chemicals through utilizing microorganisms as microbial cell factories (Beri et al., 2020; Liang et al., 2015; Yang et al., 2020). Traditionally, this process was conducted by assembly of the target biosynthetic pathway in a single strain (Yao et al., 2013). In recent years, coculture-based engineering approaches (Arora et al., 2020; Minty et al., 2013; Stephens et al., 2019; Zhang and Wang, 2016) have emerged, where a complex synthetic metabolic pathway is divided into modules expressed in separate strains thus forming a synthetic microbial consortium (Lindemann et al., 2016) that effectively produces high-value metabolites (Honjo et al., 2019; Tsoi et al., 2019; Wang et al., 2020; Zhou et al., 2015).

The functioning of a synthetic microbial consortium often requires dedicated coordination and regulation (Di and Yang, 2019). Recently, Quorum sensing (QS) (Stephens and Bentley, 2020) has been applied in cocultivations to synchronize microbial communities (Du et al., 2020; Kong et al., 2018; Kylilis et al., 2018; Scott et al., 2017; Wu et al., 2021) and reduce the competition between cell growth and targeted production (Gupta et al., 2017; Soma and Hanai, 2015; Wu et al., 2020a). Specific QS signals such as acylated homoserine lactones (AHLs) (Papenfort and Bassler, 2016) accumulate in cell populations and induce the activation of various QS-based synthetic devices (Wu et al., 2020b), such as QS-based synchronized lysis circuit (QS-SLC) and QS-based metabolic toggle switch (QS-MTS). Combined with specific killing proteins such as CcdB (You et al., 2004) or $\phi X174 E$ (Din et al., 2016), different QS-SLCs were constructed to control the cell density of a single strain. Based on the bi-directional communication through *lux* and *las* QS systems, Balagadde et al. (Balagadde et al., 2008) developed two QS-SLCs for simulating a synthetic *Escherichia coli* predator-prey ecosystem. Scott et al. (Scott et al., 2017) combined *lux* QS-SLC with *rpa* QS-SLC to control population densities of competitive microbes of *Salmonella typhimurium* strains. To realize one-step fermentation for vitamin C, Wang et al. (Wang et al., 2019) applied a *lux* QS-SLC to control the lysis of *Gluconobacter oxydans* for L-

sorbose production in a three-species consortium. Recently, to avoid QS crosstalk, an QS-based inducible synchronized lysis circuit (iSLC) was constructed orthogonally based on *p*-coumaric acid and was verified at the community level (Miano et al., 2020).

On the other hand, QS-MTS has been successfully employed in dynamic metabolic engineering to reduce the competition between cell growth and targeted production to increase bioprocess productivity and yield of products such as isopropanol (IPA) (Soma and Hanai, 2015), poly- β -hydroxybutyrate (Gu et al., 2020), 1,4-butanediol (Liu and Lu, 2015), myo-inositol (Gupta et al., 2017), D-glucaric acid (Doong et al., 2018), salicylic acid (Dinh and Prather, 2019), and naringenin (Dinh et al., 2020). In particular, Soma et al. (Soma and Hanai, 2015) constructed a synthetic QS-MTS for the mono-cultivation of the *E. coli* strain to achieve a dynamic switch of the metabolic flux between TCA cycle and IPA synthesis pathway to increase the IPA titer. Gupta et al. (Gupta et al., 2017) and Doong et al. (Doong et al., 2018) introduced *esa* QS-MTS to identify the optimal point of switch to direct most of the glucose to the target pathway to increase titers of myo-inositol and D-glucaric acid. For the production of naringenin and salicylic acid, Dinh et al. (Dinh and Prather, 2019) integrated *lux* or *esa* QS systems and CRISPRi to accomplish the metabolic flux control in engineered *E. coli*. Recently, Wu et al. (Wu et al., 2020a) built a global resource allocation device combining the sequence-dependent endoribonuclease MazF with QS-based circuits to develop a pathway-independent and full-autonomous global resource allocation strategy in one strain, and it was verified by the titer improvement of medium chain fatty acids.

Among the targeted products, IPA is a renewable cellulosic biofuel (Walther and François, 2016) which is regarded as a potential alternative for petroleum-based transport fuels. Glycosides, on the other hand, represent a type of highly important natural products relevant to various pharmacological, food, and nutraceuticals activities (Liang et al., 2015). Salidroside, a typical glycoside, has been extensively used for treating or preventing cerebral ischemia, fatigue, hypoxia and neurodegenerative diseases (Panossian et al., 2010). To tackle the metabolic burden, products including

IPA and salidroside can be heterologously produced in a synthetic microbial coculture. With the help of a *lux* QS-SLC, Honjo et al. (Honjo et al., 2019) constructed a coculture to improve the isopropanol (IPA) titer with an engineered microbial community composed of an *E.coli* strain producing beta-glucosidase (BGL) enzyme and glucose (GLU strain) and the other *E.coli* strain producing IPA (IPA strain). Previously, to improve the titer of salidroside, we have constructed a syntrophic *E. coli* coculture with the aglycone (AG) strain and the glycoside (GD) strain for the first time producing tyrosol and salidroside, respectively (Liu et al., 2018). We found that when individually optimized strains are physically mixed and co-cultivated, the coculture might be imbalanced due to the competitive growth and metabolic stress. Selective utilization of carbon source such as the glucose and xylose could be applied for reducing the cell-cell competition (Freilich et al., 2011; Liu et al., 2018; Saini et al., 2017; Zhang et al., 2015), but it requires the dynamic and automatic regulation for the cell growth to realize the cell growth balance and sustained stability.

While QS-based circuits such as QS-SLC and QS-MTS have demonstrated their potential in synchronizing and improving the target metabolism of various strains and microbial communities, they have largely been used separately so far, which may limit their scope of application in cocultivation. Besides, existing studies have often focused on the demonstration of feasibility and potential function of a novel scheme; optimal design and selection of QS systems in connection with engineering objectives such as coexistence, titer improvement, and batch fermentation duration are yet to be further explored particularly for cocultivations.

In this work, we aim to address the above deficiencies through a combination of theoretical analysis and experimental investigation (a workflow diagram can be found in Fig. S1). We have first used existing data on IPA production and carried out *in silico* assessment of co-cultivation designs that incorporate both QS-SLC and QS-MTS implemented through a range of combinations of four QS systems (*lux*, *rpa*, *tra*, *las*). The aim is to shed light on the feasibility and optimality of such systems which simultaneously involve cell growth competition and cooperative IPA production. A

process characteristic termed “glucose split ratio” is proposed to analyze the competition between cell growth and targeted production. The impact of the initial settings such as the initial seeding ratio in cocultivation has also been evaluated on selected cases. Furthermore, for a previously unstable cross-feeding system producing salidroside, we have experimentally constructed the combinations of QS-SLC, QS-MTS, and other control modules and manipulated the initial operational settings for the first time to regulate the cell growth competition, realize the growth balance of strains, and improve the production titer. Overall, this study is to shed light on the potential significance of optimal selection and combination of QS devices in the engineering of synthetic microbial communities for producing valuable products.

2. Material and methods

2.1 Mathematical modelling development for IPA case

The complete models for GLU or IPA individual strain mono-cultivation are given in Sections 1.2 and 1.3 of supplementary material; the model development for cocultivations of GLU and IPA strain is shown in Sections 1.4 to 1.6 of supplementary material; here a brief summary is provided. Four QS systems commonly used in recent studies (*lux* QS (Miller and Bassler, 2001), *las* QS (Sandoz et al., 2007), *rpa* QS (Scott et al., 2017)) and *tra* QS (Vannini et al., 2002) were investigated in this work. The QS model was based on previous work (Balagadde et al., 2008; Honjo et al., 2019; Scott et al., 2017; Scott and Hasty, 2016; Soma and Hanai, 2015; Song et al., 2009), with important parameters (identified by a sensitivity analysis, Table S2) calibrated in this work from data of Scott et al (Scott and Hasty, 2016) (listed in Table S3). In general, the behavior of a QS system (and hence the values of its kinetic parameters) may vary with the settings of its host organism and growth conditions in a non-ideal environment (Mukherjee and Bassler, 2019). In this work, fixed parameter values for each QS device are adopted, similar to previous studies of QS system selection for synthetic microbial consortia (Kylilis et al., 2018; Scott and Hasty, 2016), based on the premise that these parameter values are representative of the differing characteristics of the four QS systems considered in this work and that the fluctuations of the parameter values would

not diminish the characteristic difference between these QS systems when they are compared within the same application implemented in a well-mixed and controlled bioreactor. Parameters of the other parts of the models, such as the growth kinetics, BGL enzyme excretion, cellobiose decomposition and IPA production were obtained by calibrating the models against the experimental data including monoculture of the GLU strain with QS-SLC (Table S1) and the IPA strain with QS-MTS (Table S4) as well as cocultivation of QS-SLC GLU strain and IPA strain without MTS (Table S5). For cases where experimental data were available, the resulting models agreed well with the literature data (Fig. S2; Fig. S3; Fig. S4), which thus formed a basis for combining the relevant model components to simulate the new cocultivation cases. We list some typical ODE equations in cocultivation of the GLU strain with QS-SLC and the IPA strain with QS-MTS for cell growth and QS mechanisms as follows (see supplementary material for more details):

Cell (GLU strain-C1, IPA strain-C2) growth and death:

$$\frac{dC_1}{dt} = g_{lg}C_1 - \frac{C_1 + C_2}{C_m} \frac{A^Z}{A_c^Z + A^Z} d \times C_1 \quad (1)$$

$$\frac{dC_2}{dt} = F \times g_{2g}C_2 - \frac{C_1 + C_2}{F \times C_m} \frac{A^Z}{A_c^Z + A^Z} d \times C_2 \quad (2)$$

QS in the GLU strain:

$$\frac{dA}{dt} = g_{aq} + a_{q^*} \times \frac{A^Z}{A_c^Z + A^Z} \frac{C_1}{C_m} - g_A \times A - 2r \times A^2 \times R^2 + 2g_{AR} \times AR \quad (3)$$

$$\frac{dR}{dt} = v_R \times C_1 - g_R \times R - 2r_R \times R^2 \times A^2 + 2g_{AR} \times AR \quad (4)$$

$$\frac{dAR}{dt} = r_R \times R^2 \times A^2 - g_{AR} \times AR \quad (5)$$

We assumed that the two QS systems are completely orthogonal with no crosstalk.

Models for the QS in the IPA strain:

$$\frac{dA_2}{dt} = g_{a_{q2}} + a_{q2^*} \times \frac{A_2^{Z_2}}{A_2^{Z_2} + A_2^{Z_2}} \frac{C_2}{C_m} - g_{A2} \times A_2 - 2r_2 \times A_2^2 \times R_2^2 + 2g_{AR2} \times AR_2 \quad (6)$$

$$\frac{dF}{dt} = \frac{K_d}{(K_d + [A])} \frac{C_1}{C_m} \frac{A^Z}{A_c^Z + A^Z} \frac{C_2}{C_m} \frac{A_2^{Z_2}}{A_2^{Z_2} + A_2^{Z_2}} \frac{C_2}{C_m} - g_{A2} \times A_2 - 2r_2 \times A_2^2 \times R_2^2 + 2g_{AR2} \times AR_2 \quad (7)$$

$$\frac{dR_2}{dt} = v_{R2} \times C_2 - g_{R2} \times R_2 - 2r_{R2} \times R_2^2 \times A_2^2 + 2g_{AR2} \times AR_2 \quad (8)$$

$$\frac{dAR_2}{dt} = r_{R2} \times R_2^2 \times A_2^2 - g_{AR2} \times AR_2 \quad (9)$$

The concentration changes of cellobiose, glucose, and IPA:

$$\frac{dE_{BGL}}{dt} = b_{BGL1} \times \frac{A^Z}{A_c^Z + A^Z} \times d \times C_1 \quad (10)$$

$$\frac{dS_C}{dt} = - \frac{k_B \times E_{BGL} \times S_C}{K_{M,B} + S_C} \quad (11)$$

$$\frac{dG}{dt} = 2 \times \frac{k_B \times E_{BGL} \times S_C}{K_{M,B} + S_C} - F \times V_M \times \frac{G}{K_{M,G} + G} \times C_2 - V_{IPA} \times \frac{G}{K_{IPA,G} + G} \times C_2 \quad (12)$$

$$\frac{dIPA}{dt} = \frac{V_{IPA} \times G}{K_{IPA,G} + G} \times C_2 \quad (13)$$

where the parameters descriptions and values are listed in Table S1-S6 in the supplementary material.

2.2 Comparison and analysis of metabolic control designs in individual strains

The purpose of this part of work was to predict the relative performance of alternative devices applied to the GLU strain or the IPA strain, thus shedding light on their optimality with respect to the respective engineering objectives.

QS-SLC was introduced in the GLU strain to control the release of the BGL enzyme, where the engineering objective can be considered as the shortening of the time needed to convert cellobiose to glucose. Using the model of the GLU strain incorporating QS-SLC (Supplementary material, Section 1.2.1), we evaluated four QS systems, namely *lux*, *las*, *rpa*, and *tra*, and compared them with a theoretical optimal lysis curve (Detailed computation approach is described in the Supplementary material, Section 1.2.2).

For the MTS in the IPA strain, the primary objective was considered to be the maximization of IPA titer, while the batch duration was also taken into account. In order to investigate glucose redirection by the MTS in the IPA strain which would dictate IPA titer, we particularly analyzed the glucose split ratio termed r_2/r_1 , where r_1 and r_2 refer to the glucose flow into cell growth and maintenance and that into IPA production, respectively. Based on the mathematical models of the IPA strain (Supplementary material, Section 1.3), r_2/r_1 follows:

$$r_2 / r_1 = \frac{V_{\text{IPA}}}{a V_{\text{M}}} \times \frac{K_{\text{M,G}} + G}{K_{\text{IPA,G}} + G} \quad (14)$$

where V_{M} and V_{IPA} are the maximum specific glucose consumption rate by (a) cell growth and maintenance and (b) IPA production, respectively; G is the glucose concentration; $K_{\text{M,G}}$ and $K_{\text{IPA,G}}$ are glucose consumption affinity of (a) cell growth and maintenance and (b) IPA production, respectively. Finally, a ($0 \leq a \leq 1$) represents the extent of reduction of glucose consumption by cell growth and maintenance due to MTS. For QS-MTS, a materializes in the fraction of the GltA enzyme (represented by the variable F in the model, see Supplementary material, Section 1.3) to describe the molecular mechanism. The same four QS systems assessed in QS-SLC for the GLU strain were modelled in QS-MTS of the IPA strain, each effecting the control through a distinct time trajectory of a .

2.3. Reagents and instruments

We purchased the standard sample of tyrosol (98% purity) and salidroside (98% purity) from Xiensiaopude Biotech (Beijing, China) and cheMart Biotech (Tianjin, China), respectively. DNA manipulating agents, including restriction endonucleases and T4 DNA ligase were obtained from New England Biolabs. DNA Polymerase of Phanta Super Fidelity and Taq for polymerase chain reaction (PCR) were purchased from Vazyme (Nanjing, China). Various plasmid kits were purchased from Tiangen Biotech (China). PCR primers were synthesized by GENEWIZ (Suzhou, China). More details for the reagents and instruments used in this study are listed in Table S10.

2.4. Plasmids and strains construction

The bacterial strains, plasmids, and primers used in this study are listed in Table S11, Table S12, and Table S13, respectively. Codon-optimized genes, including *ccdA*, *ccdB*, BGL enzyme gene, and series genes of *lux* QS, *rpa* QS systems were fully synthesized by GENEWIZ (Suzhou, China). For the p15AT0, the p15A ori, *lac* promoter, and the *ccdB* gene were inserted into petDuet-1, a vector containing the repressor for the tac promoter *lacI*, using restriction digestion with XbaI and Hind III. Similar to p15AT0, series of genes were inserted into petDuet-1 to be p15AT1, p15AT2,

p15AT3, and p15AT4 illustrated as Fig. S11. We used XbaI and HindIII restriction endonucleases to cut plasmid pLX2 (from our previous study, (Liu et al., 2018)) and connected the BGL enzyme gene and the tyrosol biosynthesis gene (*synkdc4*) with a seamless cloning kit to be the pLX2 BGL plasmid (Fig. S11). After the connection, primer pLX2YZ-1 and pLX2YZ-2 (Table S13) were used for colony PCR verification. In addition, series of genes, such as *tetR* and *citA*, were connected and inserted into the petDuet-1 to be p15AS1 and p15AS2 listed in Fig. S12. Expression plasmids were confirmed by enzymatic digestion and DNA sequencing, and then transformed into *E. coli*, generating engineered strains. Based on our previous study (Liu et al., 2018), *E. coli* BW25113 derivatives were used to construct the AG strains (BMT21 and BMT23 strain) for tyrosol biosynthesis, and *E. coli* BL (21) was used to construct the GD strain (BMS24 strain) for salidroside production.

2.5. Culture media and conditions

We applied the Luria broth (LB) medium to maintain strains and prepare seeds. All batch fermentations for salidroside, including mono-culture and coculture, were carried out in M9 medium containing 17.1 g/L Na₂HPO₄·12H₂O, 3.0 g/L KH₂PO₄, 0.5 g/L NaCl, 1.0 g/L NH₄Cl, 5mM MgSO₄, 0.1mM CaCl₂, supplemented with desired amounts of various combinations of glucose, xylose, and cellobiose. Trace elements were also supplemented to the media, giving final concentrations of 0.4 mg/L Na₂EDTA, 0.03 mg/L H₃BO₃, 1 mg/L thiamine, 0.94 mg/L ZnCl₂, 0.5 mg/L CoCl₂, 0.38 mg/L CuCl₂, 1.6 mg/L MnCl₂, and 3.6 mg/L FeCl₂. In addition, 50 mg/L phenylalanine and tyrosine were supplemented to the coculture to feed the AG and GD strains which are amino acid deficient strains. Antibiotics (20 µg/mL chloramphenicol, 50 µg/mL ampicillin, and 30 µg/mL streptomycin) were supplemented to the medium when needed. IPTG was added into the medium at a different time and different final concentration when needed. Various ratios of glucose and xylose (1:1, 2:1, 4:1, and 6:1) were tried to have a greater salidroside titer. The total addition of glucose and/or xylose is 10 g/L. Cellobiose addition (5 g/L) and different initial cell density of AG and GD strains (1:1, 1:2, 1:4, 1:6, 1:8, and 1:10) were tried to have a greater salidroside titer.

All engineered *E. coli* strains were cultivated at 37 °C and 220 rpm shaking. The overnight cultures were diluted 1:100 into 50 mL fresh LB medium for seed preparation, and cultivated for 4–6 h, then harvested and transferred to M9 medium for fermentation at 30 °C and 200 rpm shaking. OD₆₀₀ and titers of tyrosol and salidroside are tested by sampling every 12h. The fermentation experiments were conducted in triplicates and data were shown as the means ± S.D.

2.6. Cocultivation analysis

The ratios of the AG and GD strains in the cocultivation were calculated by their phenotypes. The fermentation broth was withdrawn and centrifuged periodically. The strains were washed with sterile water three times, appropriately diluted and plated on M9 medium plus 50 mg/L of phenylalanine or tyrosine with glucose or xylose as the sole carbon source. The plates were then incubated at 37 °C for growth. We counted the colonies on each plate (100–500 colonies each plate) and estimated the ratios of AG and GD strains.

2.7. Biomass and metabolite analysis

We measured the cell optical density (OD) at 600 nm with TU-1810 spectrophotometer. We measured the residual glucose concentration in the cocultivation medium by a biosensor SBA-90 (Biology Institute of Shandong Academy of Sciences, China). We applied the Agilent 1200 HPLC system equipped with a C18 column (250 * 4.6mm with a particle size of 5 µm, Bonna-Agela, China) and a PDA detector (Agilent) to measure the concentration of the tyrosol, salidroside, and other metabolites. The fermentation samples were centrifuged, and the cell-free culture supernatants (20 µL) was filtered through pore-sized syringe filters (0.22 µm) before being measured at 225 nm under room temperature with a mobile phase (20% methanol, 80% water, 0.1% acetate) at 1 mL/min. With R² coefficient for the calibration curve being higher than 0.99, we conducted and quantified the titers of tyrosol and salidroside every 12 h by using five-point calibration curves.

3. Results

3.1 IPA production

Presenting the mathematical modelling results of the IPA production case, this section begins with the GLU strain monoculture with a focus on the comparison between the model-predicted performance of four different QS systems implementing the lysis control (Section 3.1.1). A similar comparison is subsequently presented to the IPA strain monoculture equipped with different implementations of QS-MTS (Section 3.1.2). Finally, GLU-IPA co-cultivation regulated with a variety of QS schemes is evaluated in Section 3.1.3.

3.1.1 Modelling for GLU strain with QS-SLC

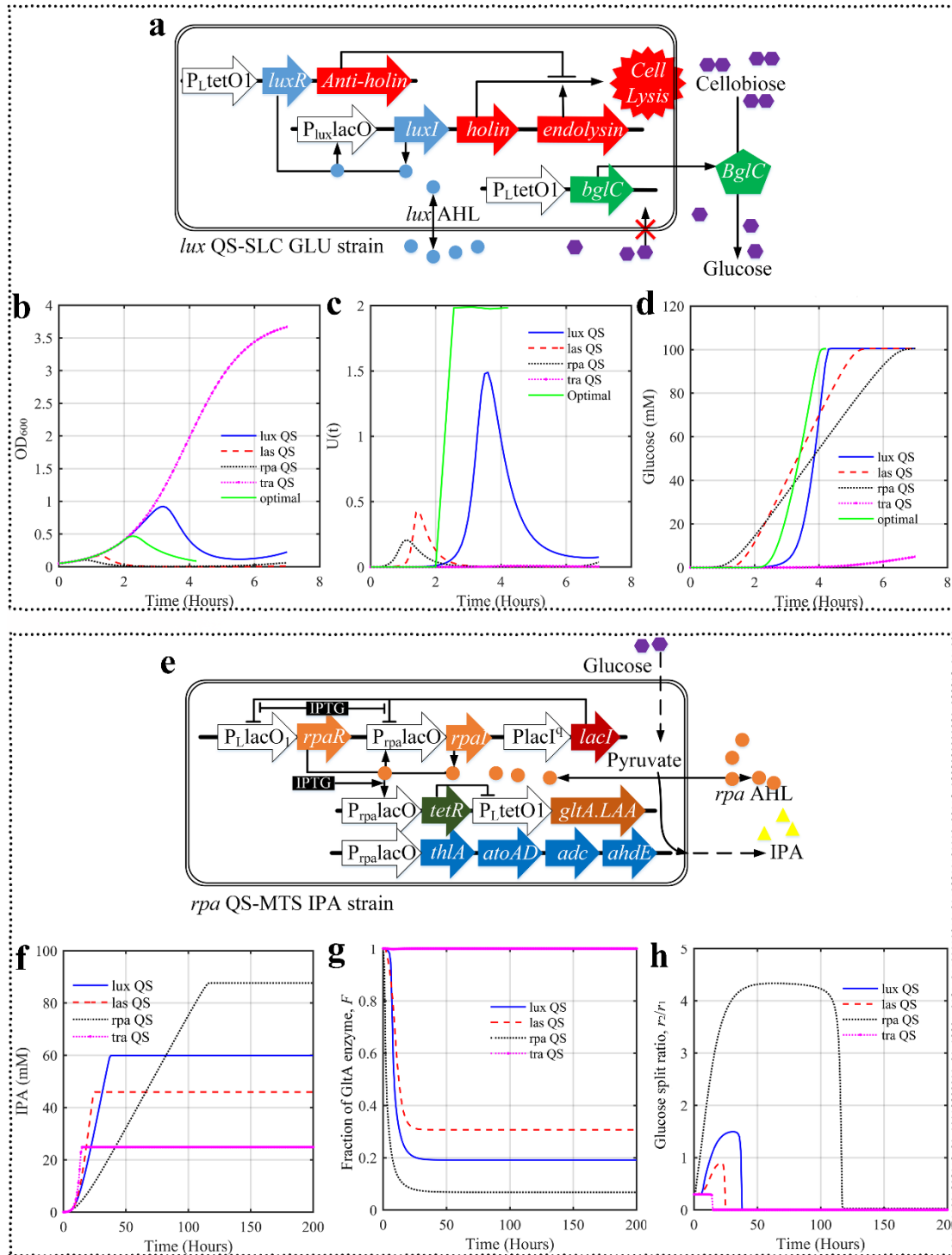
In the strain producing glucose from cellobiose (GLU strain), a QS-SLC was applied to regulate cell lysis to release the intracellularly accumulated BGL enzyme once the cell density has reached a suitable level (Fig. 1a). Using the model (Supplementary 1.2) calibrated with the experimental data from Honjo et al. (Honjo et al., 2019), we simulated the cell density, cellobiose, and glucose concentration and obtained good agreement with the experimental results (Fig. S2). Simulations with the common four QS systems (*lux*, *las*, *rpa*, and *tra*) showed that except the case with *tra*, the QS-based synchronized lysis circuit is effective in controlling the cell density of the GLU strain (Fig. 1b). The lysis curves realized by the four QS systems are shown in Fig. 1c, in comparison with the theoretical optimal lysis curve computed for minimizing the cellobiose-to-glucose conversion time (Supplementary 1.2.2). The time required for the complete conversion is the shortest with *lux* (4.3 h), followed by *las* (5.7 h), *rpa* (7 h) and *tra* (end point not simulated) (Fig. 1d). The poor performance of the *tra* QS-SLC was because the production rate of the QS signal molecule in *tra* is lower than that of other QS systems (Table S3). The theoretical minimum time for glucose accumulation is 4.1 h, which suggests that the *lux* QS-SLC, the one adopted in the experimental study of Honjo et al. (Honjo et al., 2019), was a superior choice. Compared to the other two QS systems (*rpa* and *las*) which can also function, the *lux* QS system results in a higher cell density threshold (Fig. 1b) and is thus able to accumulate more BGL enzyme in the GLU strain. This turns out to be advantageous: despite a later start of glucose accumulation, the GLU strain with *lux* QS-SLC enjoys a faster glucose accumulation

rate due to the higher BGL enzyme concentration and eventually reaches the peak glucose concentration in the shortest time (Fig. 1d).

3.1.2 Modelling for IPA strain with QS-MTS

Using the model (Supplementary 1.3) calibrated with the experimental data from the culture of the IPA strain with *lux* QS-MTS (Fig 1e) reported by Soma et al.(Soma and Hanai, 2015) (Fig. S3), four QS systems were simulated for comparison (Fig. 1f-h). Among the four QS systems, the order of IPA titer ($tra < las < lux < rpa$) (Fig. 1f) is the reverse of that of glucose consumption rate. The correlation between a slower glucose consumption and a higher IPA titer can be explained by the glucose split ratio between cell growth and IPA production (see Methods) (r_2/r_1 , Fig. 1h) which in turn is affected by the fraction of GltA enzyme (F , Fig. 1g). F always decreases from 1, however at different paces depending on the QS systems applied. According to equation 14, r_2/r_1 is dictated by and is (approximately) inversely proportional to F (in the case of QS-MTS) when glucose concentration is high, which occurs at the early stage of a batch. Fig. 1g shows that among the four QS-MTS options, *rpa* leads to the fastest decline in F which eventually stabilizes at the lowest level. Consequently, its r_2/r_1 rises most rapidly and reaches the highest value, implying the greatest fraction of glucose channeled to IPA production (Fig. 1h). On the other hand, the most rapid dropping of F with the *rpa* QS-MTS leads to the most severely limited growth of cells and thus the longest time to convert glucose. The *tra* QS-MTS is at the other extreme, with the slowest dropping in F leading to the fastest consumption of glucose, the lowest r_2/r_1 and hence the lowest IPA titer; between *rpa* and *tra* lie the other two QS systems, *lux* and *las*. From Fig. 1h, one can see that after F reaches a lowest value, r_2/r_1 will stabilize for a period of time while it remains to be dominated by F , until the depletion of glucose eventually makes the residual glucose concentration the dominating factor and causes a rapid decline of r_2/r_1 as glucose is being completely consumed (Supplementary 1.3). This later stage of development, where an increase is predicted of glucose consumption by the growth and maintenance of the cells, does not play a significant role in shaping the overall distribution of glucose between meeting the demand of the cells and IPA

352 production throughout the batch.



353
 354 Fig. 1. Model-predicted comparison of QS systems in the GLU (upper box)
 355 strains with QS-SLC and QS-MTS, respectively. (a) Schematic diagram of the *lux* QS-SLC GLU
 356 strain (Honjo et al., 2019) to illustrate the QS-SLC structure. *lux* AHL is produced with the help of
 357 the protein LuxI; when the concentration of AHL reaches a certain threshold, it binds to the LuxR
 358 protein to form a dimer complex to activate the expression of lytic genes *holin* and *endolysin*
 359 derived from T4 phage to promote the lysis of the GLU strain and the release of the BGL enzyme.

(b)-(c) Time course of cell density and cell lysis (with “ U ” denoting the lysis intensity, see Supplementary material, Equation S10) of the GLU strain. (d) Time course of glucose concentration in the medium; (e) Schematic diagram of the *rpa* QS-MTS IPA strain (Soma and Hanai, 2015). When a desired cell density of IPA strain is reached, the binding dimer complex of *rpa* AHL and RpaR receptor activate the expression of *tetR* to inhibit the *gltA* transcription, and activate the *rpa* QS-MTS at the same time; (f)-(h) Time course of IPA concentration, F , and r_2/r_1 with *lux*, *las*, *rpa*, and *tra* QS-MTS.

3.1.3 Modelling for cocultivations of GLU and IPA strain

The investigation here started with cocultivation of an engineered glucose producing (GLU) strain with a *lux* QS-SLC and IPA producing (IPA) strain without MTS, for which experimental data is available (Honjo et al., 2019). With 10 g/L cellobiose as the substrate, the modelling results for this cocultivation with a *lux* QS-SLC (Supplementary 1.4) agreed well with the experimental data from Honjo et al. (Honjo et al., 2019) (Fig. S4). Using the model, we also simulated the cocultivation with *las*, *rpa*, and *tra* QS-SLCs. Fig. 2a shows close performance of QS-SLC with *las* and *rpa*. The case with *lux*, on the other hand, leads to a slower degradation process. Unlike in the monoculture case presented above, the higher level of accumulated BGL enzyme caused by its higher cell density in this case does not lead to higher acceleration in degradation due to the lower initial concentration of cellobiose (10 g/L) than the former monoculture case (20 g/L). However, all the strategies except that that with *tra* (which suffers from a slow lysis rate, as pointed out earlier) are predicted to result in a similar IPA titer (Fig. 2c). As there is not MTS in the IPA strain, glucose split ratio r_2/r_1 is determined only by glucose concentration (cf. Equation 14). Fig. 2d shows that the r_2/r_1 curves are similar for the designs with *rpa* and *las*, which are consistent with the similar glucose trajectories shown in Fig. 2b. The *lux*-based strategy, which takes a longer time to degrade cellobiose, also leads to a similar IPA titer, as it shares a similar overall history of r_2/r_1 (and glucose concentration) throughout the batch despite the shift caused by the later start of lysis.

A comparison between r_2/r_1 in the above cocultivation (Fig. 2d) and that of the monoculture case of the IPA strain with MTS (Fig. 1h) points to the great potential of

introducing MTS into cocultivation to better direct glucose to IPA production, which
 was further studied by an extended co-cultivation model (Supplementary 1.5). Here,
 the QS-SLC (“QS1”) GLU strain is cocultured with the IPA strain with QS-MTS “QS2”
 to produce IPA (denoted below as “QS1/QS2”). We assume that the two QS systems
 used in QS-SLC and QS-MTS are orthogonal (Kylilis et al., 2018). Adopting the same
 initial cell densities (Table S7) and the same initial cellobiose concentration as in the
 cocultivation simulations presented above, we predicted the final IPA titers and the
 corresponding fermentation times for 12 possible combinations of two-QS
 cocultivation, with results listed in Table S8. Fig. 2e-2h shows further details of one of
 the most productive combinations, *las/rpa*, and one of a medium IPA titer, *lux/las*. The
 key difference between the two combinations appears to lie in the more rapid MTS
 action of *rpa* than *las*, which leads to the rapid reduction in F (fraction of GltA enzyme)
 (Fig. 2g) and consequently significantly higher r_2/r_1 in *las/rpa* (Fig. 2h). As more
 glucose is channeled to IPA production, although the conversion rate is lower compared
 to *lux/las*, the IPA titer eventually achieved by *las/rpa* is significantly higher (Fig. 2f).
 At the same time, its slower glucose consumption (Fig. 2e), caused by the limited cell
 density of the IPA strain due to the MTS, does mean a prolonged batch duration (Fig.
 2f). These results show again that the attainable IPA titer depends on how QS-regulated
 co-cultivation scheme dictates the glucose split ratio (r_2/r_1) between IPA production and
 meeting the cellular needs.

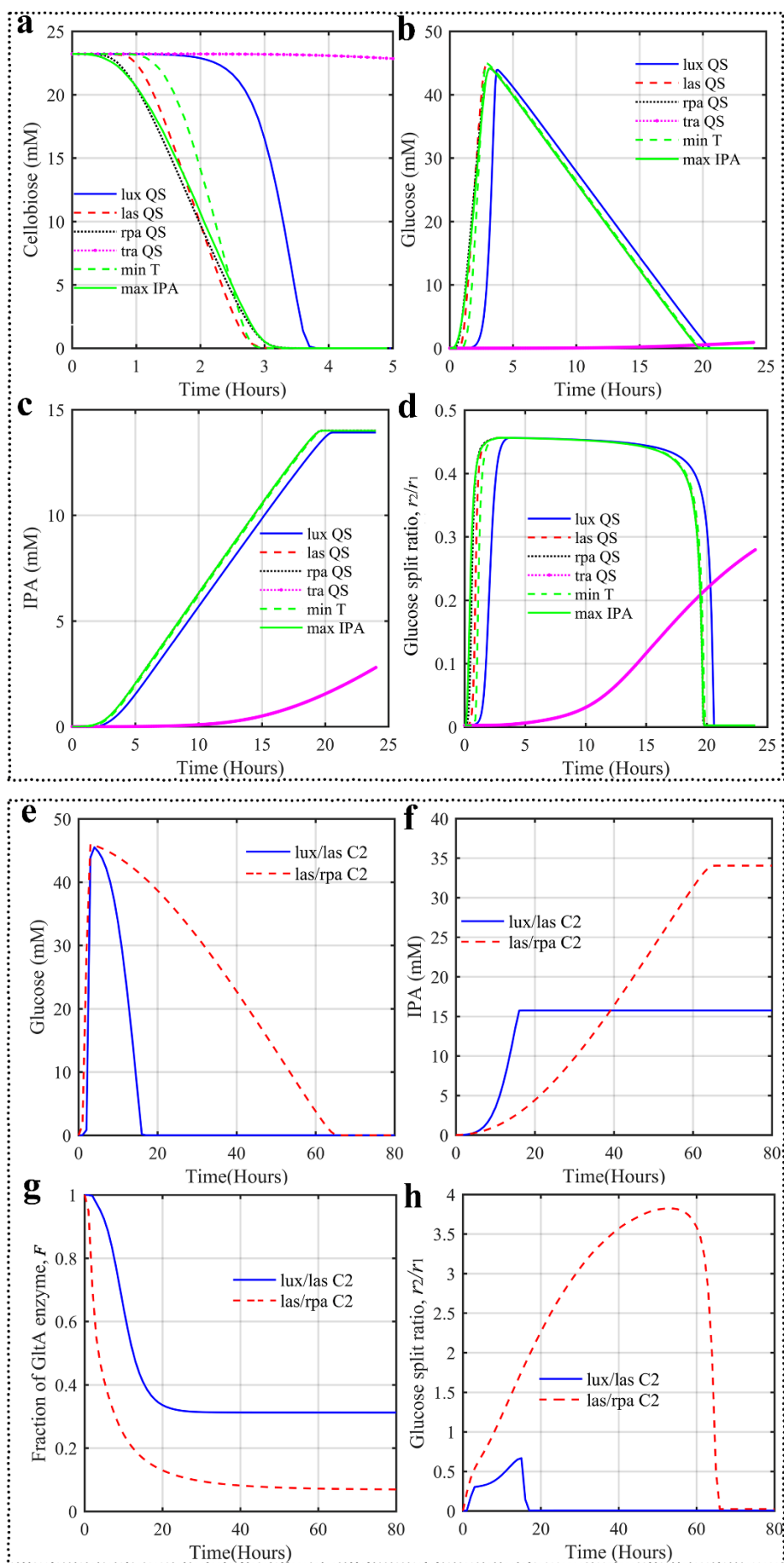


Fig. 2. Model-predicted comparison between different QS-regulated schemes for cross-feeding cocultivations of GLU and IPA strains with QS-SLC only (upper box) and with both QS-SLC and QS-MTS (lower box). (a)-(d) The dynamic characteristics of no QS-MTS cocultivations with four QS-SLCs control strategies in GLU strain; (e)-(h) The comparison for *lux/las* and *las/rpa* cocultivations.

3.2. Salidroside production

The above simulation results on IPA cases suggest that the combination of QS-SLC (QS-based synchronized lysis circuit) and QS-MTS (QS-based metabolic toggle switch) can be designed to realize the regulation of growth competition and production cooperation in the cross-feeding cocultivations. Encouraged by this learning, we introduced such control in a coculture system for producing salidroside with a cross-feeding structure similar to that of the IPA case (Fig. 3) where, on the other hand, achieving the coexistence of the cross-feeding strains was particularly challenging. This experimental syntrophic *E. coli* coculture was composed of an aglycone (AG) strain and a glycoside (GD) strain for producing tyrosol and salidroside, respectively. QS-based cell killing (not lysis, which however is still termed as “QS-SLC” in this case to facilitate the cross reference with corresponding device used in the IPA case that plays a similar role) was introduced to the AG strain to regulate the cell population, tyrosol production (the intermediate glycoside for salidroside), and the release of BGL enzyme that converts the cellobiose to glucose; the experimental results are presented in Section 3.2.1). An MTS module was made available to the GD strain to reduce the competition between cell growth and targeted production to increase the titer of salidroside, with results reported in Section 3.2.2. Finally, the results of co-cultivation of both engineered strains for producing salidroside are presented in Section 3.2.3.

3.2.1 Engineering AG strains with different QS-SLCs

Two AG strains (BMT21: using glucose as the carbon source; BMT23: utilizing xylose preferentially due to the deletion of the *manZ* gene; see Table S11 for details of all strains) were tested with the view to produce tyrosol as the precursor for synthesizing salidroside in a co-cultivation. Aiming to control the growth of the AG strains (Fig. 3,

upper), we constructed four QS-SLC modules (killing-first, antikilling-first, CI-based, and TetR-based QS-SLC modules) in four plasmids (p15AT1, p15AT2, p15AT3, and p15AT4, listed in Table S12) through combinations of CcdB, CcdA (Balagadde et al., 2008) (antidote protein to act against CcdB), and two repressor proteins (CI (Elowitz and Leibler, 2000) and TetR (Liu et al., 2019)). For both AG strains, the cell density (OD_{600}) achieved in monoculture with any of the four QS-SLC modules was lower than without the QS-SLC module (Fig. S9). In addition, we equipped each AG strain with the expression of the beta-glucosidase (BGL) enzyme which would be released by cell killing to produce additional glucose for the GD strain, thus improving the salidroside titer.

As illustrated in Fig. 4a and Fig. S9c, cell densities of the BMT23 strains with (BMT23T1B - BMT23T4B) or without BGL enzyme (BMT23T1 - BMT23T4) can be controlled effectively with 5 g/L xylose as the carbon source. Note that cell killing control for BMT23T2B (with antikilling-first QS-SLC) was better than BMT23T1B (with killing-first QS-SLC) with 5 g/L xylose and 5 g/L cellobiose as the carbon source (Fig. 4b). This indicates that the expression sequence of CcdA and CcdB has different effects on cell killing control. For BMT23T1B with killing-first QS-SLC, when the antidote protein CcdA is expressed later than CcdB, the cell killing control can fail due to the cumulation of CcdA as fermentation continues, which leads to the increase of cell density, thus consuming glucose from decomposing cellobiose. The glucose concentrations in the medium for culturing BMT23T2B-T4B, increased gradually (Fig. 4c), and reached about 3 g/L at 48 h, which is beneficial for the regulation of the growth competition and hence the cooperation with the GD strain when co-cultured for salidroside production. Cell killing control achieved with BMT23T3B (with a CI-based QS-SLC) and that with BMT23T4B (with a TetR-based QS-SLC) were similar, indicating insignificant difference between CI and TetR repressors for cell killing control. In addition, because part of the glucose from cellobiose degradation can be utilized by the AG strains, higher tyrosol titers were achieved with the combined use of xylose and cellobiose as the carbon source than xylose alone (Fig. 4d).

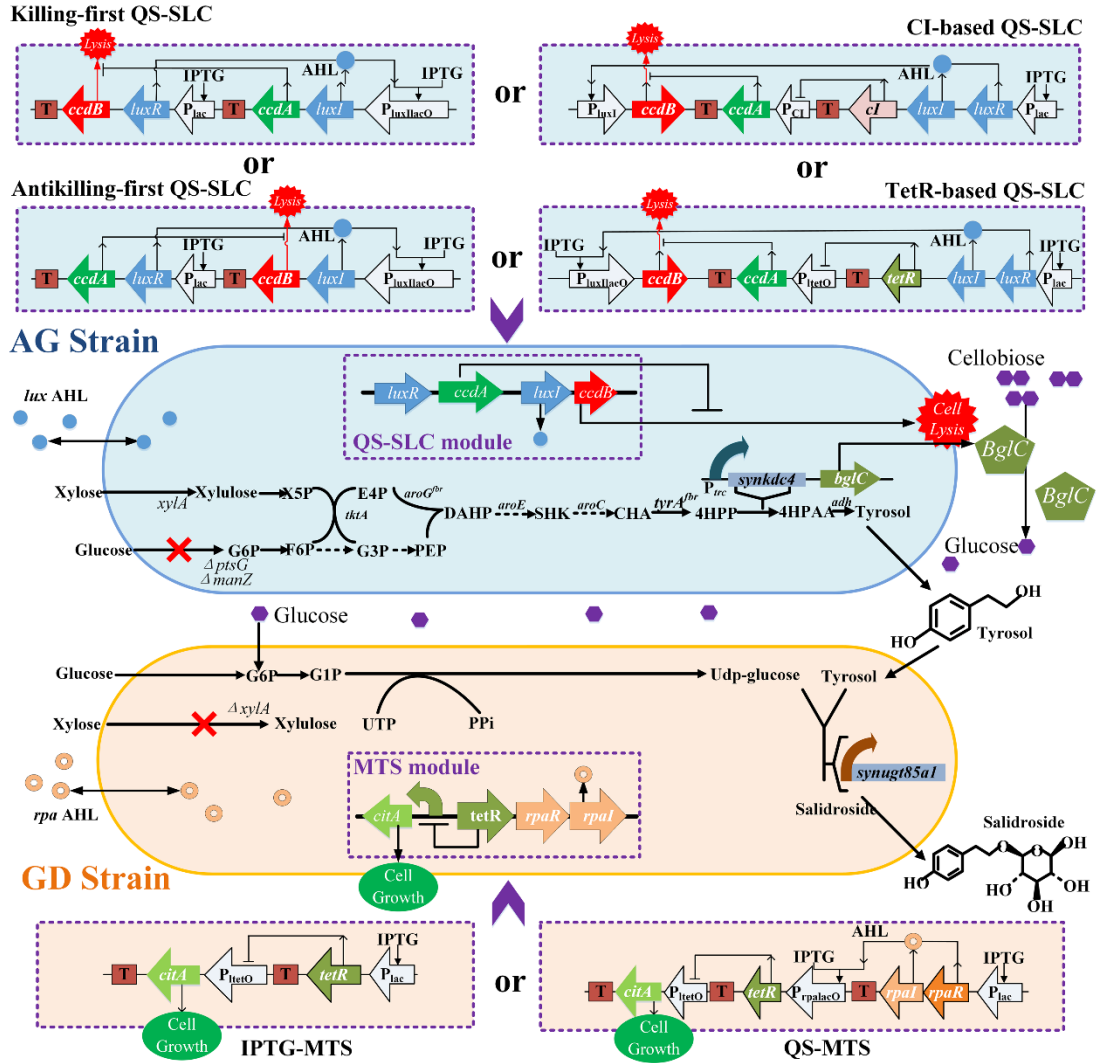


Fig. 3. Cocultivations of engineered AG and GD strains with combinational QS devices for salidroside production. For an AG strain with a killing-first QS-SLC module, when the concentration of *lux* AHL is low at a low cell density, CcdB will be induced by IPTG. As the cell density increases, *lux* AHL accumulates and binds to LuxR to become a complex which promotes the expression of CcdA to act against CcdB, and vice for the expression sequence of CcdA and CcdB in the antikilling QS-SLC module. For an AG strain with CI-based or TetR-based QS-SLC module, CcdA will be induced by IPTG at a low cell density. When the population reaches the critical threshold, the complex of *lux* AHL and LuxR will promote the expression of CI/TetR repressor protein as well as CcdB to decrease the expression of CcdA and activate cell killing.

Either an IPTG induced MTS (IPTG-MTS) or a QS-based MTS (QS-MTS) is used in the engineered GD strain. In this scenario, *citA* encodes citrate synthase, which is expressed at the early growth stage to enhance the TCA cycle and accelerate strain growth. When a desired cell density of the GD strain is reached, the MTS will be activated by stopping the heterologous expression of *citA*, thus channeling more carbon source to salidroside production.

3.2.2 Engineering GD strains with MTS

We designed and constructed a metabolic toggle switch (MTS), induced by IPTG (IPTG-MTS) or the *rpa* QS system (*rpa* QS-MTS), to regulate the competition between cell growth and targeted production to maximize the salidroside titer (Fig. 3, lower). Compared to the original BMS24 strain, higher cell densities (OD₆₀₀) were achieved by BMS24 with an IPTG-MTS (BMS24S1) and BMS24 with a QS-MTS (BMS24S2) after 24h (Fig. 4e). With 0.5 g/L tyrosol and 5 g/L glucose, the salidroside titers at 48h of BMS24S1 and BMS24S2 were 1.197 g/L and 1.093 g/L, respectively, which are 36.17% and 24.35% greater than that of BMS24 (0.879 mg/L) (Fig. 4f). This indicates that the production of salidroside could be effectively improved by a MTS device in the GD strain, which is thus a promising option to be adopted in a cocultivation system.

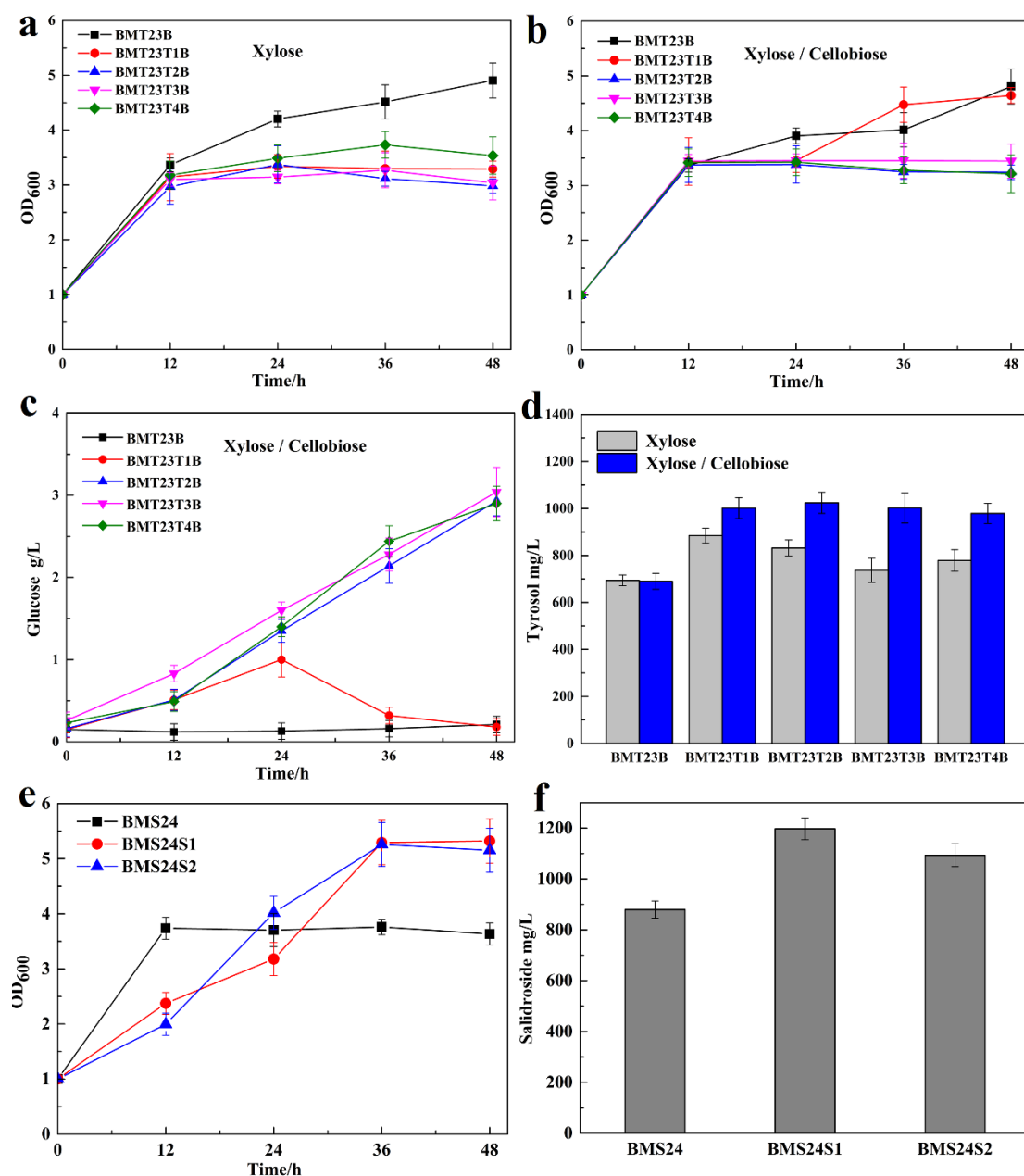


Fig. 4. Comparisons of the engineered AG strains or GD strains mono-cultivations. (a)-(b) Time course of the cell density (OD_{600}) of AG strains using xylose (10 g/L) with or without cellobiose (5 g/L); (c) Time course of cell densities and glucose concentrations of AG strains with xylose (10 g/L) and cellobiose (5 g/L); (d) Tyrosol titer comparisons for the mono-cultivations of AG strains using xylose with or without cellobiose at 48h; (e)-(f) Cell densities (OD_{600}) and solidoside titers (mg/L) for GD strain mono-cultivations with glucose (10 g/L) and tyrosol (0.5 g/L).

3.2.3 Cocultivations of AG and GD strains

After completing the engineering of AG strains and GD strains, we have tested a wide range of cocultivation combinations in terms of the regulation measures adopted for one or both strains and the options for utilizing carbon sources, which are listed in

Table S14 with a subset shown in Fig. 5a. All these tests were with an initial AG/GD strain ratio of 1/1 and, where xylose was added, the initial ratio of glucose/xylose of 1/1 (Table S14). Without the utilization of xylose, the engineering of either or both strains produced titers lower than the control case, suggesting their failure in improving the growth balance between the two strains and possibly a negative effect of the metabolic burden introduced by the engineered devices. The same ineffectiveness of the engineered strains can also be observed from comparing (a) the co-culture cases utilizing both glucose and xylose with the engineering of one or both strains (BMT23+BMS24S2, BMT23B+BMS24S2, and BMT23T2+BMS24S2) and (b) that without using engineered strains (BMT21+BMS24). On the other hand, the combination of xylose utilization, BGL expression, cellobiose degradation, and an antikilling-first QS-SLC module for BMT23 (BMT23T2B) showed a rather positive outcome when cocultured with BMS24, improving the salidroside titer by about 62% from the control case (BMT21+BMS24) and about 13% from the case with xylose utilization by the BMT23+BMS24 case (Fig. 5a). This suggests that the additional glucose available from cellobiose degradation can provide extra energy that would sufficiently compensate for any metabolic burden introduced by the engineering of the AG strain and eventually promote the growth of the GD strain and its production of salidroside.

Encouragingly, the best performance was demonstrated by the combined use of both engineered strains and all the carbon sources (BMT23T2B+BMS24S2, Fig. 5a), which increased the salidroside titer by 172.1% from the control case and by 68% from the earlier-introduced second best case (BMT23T2B+BMS24) which did not incorporate MTS into the GD strain. This clearly verifies that the combinational QS devices (QS-SLC and QS-MTS) can improve the titer of the target product for a highly competitive system such as the cocultivation of AG and GD strains with the help of BGL enzyme release and cellobiose degradation. Note that there are higher salidroside titers for the cocultivations including BMS24S1 (405.5 mg/L, Table S14) than that of BMS24S2 (348.8 mg/L), which may be caused by the greater metabolic burden

introduced by the QS-related proteins from QS-MTS. In addition, Table S14 shows that a large amount of tyrosol accumulated in the cocultivation was not converted to salidroside at the end of many batches, which suggests that the initial experimental settings adopted may have room for significant optimization.

Taking the two most promising cocultivation combinations, BMT23T2B+BMS24S1 and BMT23T2B+BMS24S2, we carried out optimization of the cocultivation conditions, such as the time and concentration of IPTG addition, the glucose: xylose ratio, and the initial ratio of the engineered AG and GD strains to further improve the salidroside titer; the results for single-factor experiments are shown in Fig. S10. With the initial cell density ratio being 1:1, the percentage of BMS24 (GD percentage) in the BMT23+BMS24 cocultivation will decrease over time due to the growth advantage of BMT23 over BMS24 strain. Compared with BMT23+BMS24, there was a total cell density increase (Fig. 5b) with the glucose:xylose ratio at 6:1 or 4:1, and the cell density fraction of the GD strain in each of the two engineered cases increased by about 60% at 48h, thus realizing the desired regulation of cell growth competition (Fig. 5c).

With 1mM IPTG added at 6h, the glucose: xylose ratio being 6/1 (10 g/L), and 5g/L cellobiose, the salidroside titer at 48h of the cocultivation BMT23T2B+ BMS24S1 was about 1.13 g/L (Fig. 5d). Adjusting the glucose:xylose ratio to 4/1 while keeping all other conditions the same, a similar high salidroside titer (1.18 g/L) was achieved by BMT23T2B+BMS24S2 (Fig. 5e) which is more than 9 times of the control cocultivation (BMT21+BMS24, 128.2 mg/L). In addition, there is an increase of glucose concentration during each of these two cocultivations (Fig. 5d and 5e), resulting from the additional glucose supply from cellobiose degradation by the BGL enzyme produced and released by the AG strain.

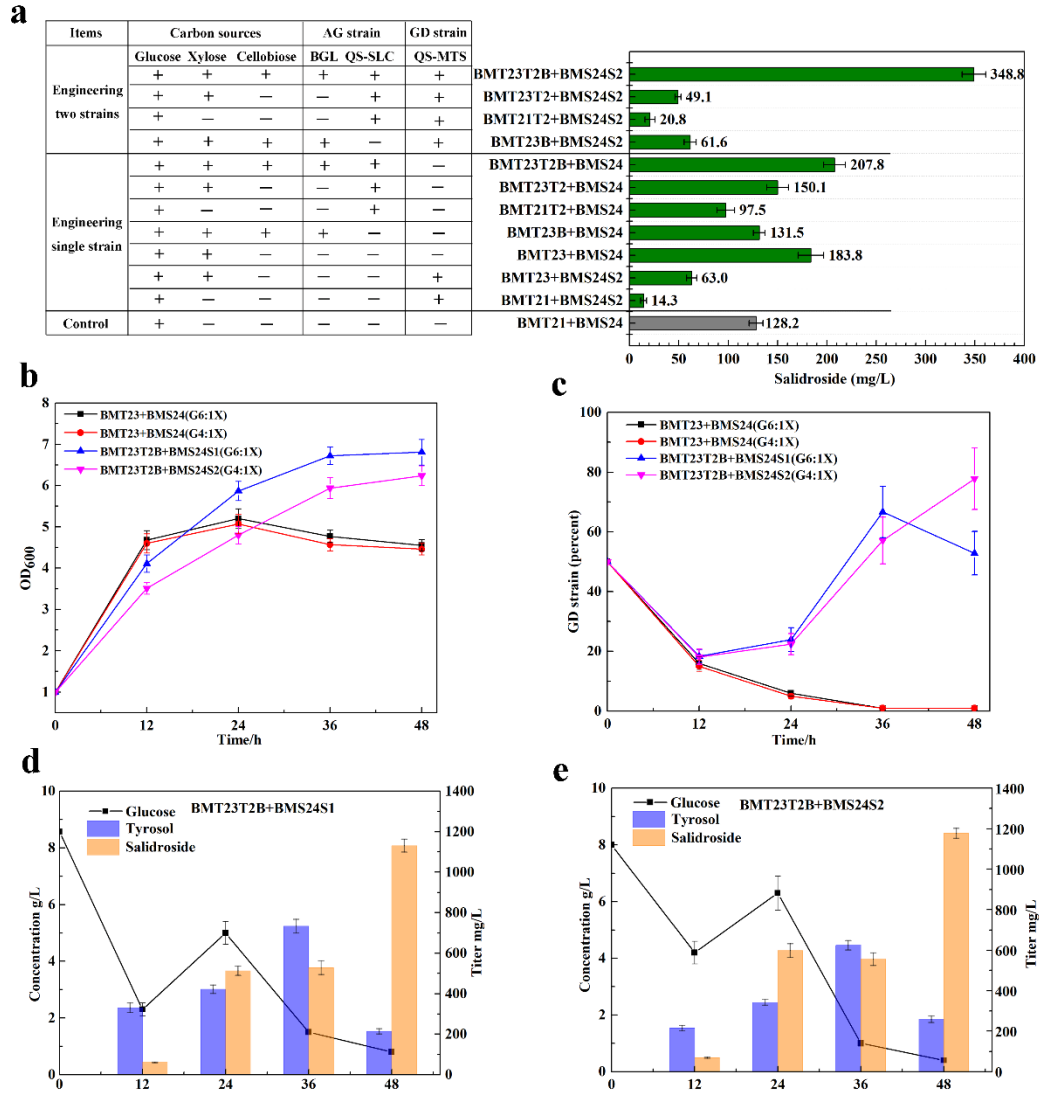


Fig. 5. Comparison of various cocultivations. (a) Salidroside titer for cocultivations including one or two engineered strains at 48h; note that “+” and “-” represent the existence and no-existence of the corresponding control strategy, respectively. Total carbon source (glucose and xylose) and cellobiose are 10g/L and 5g/L, respectively; the initial ratio of glucose/xylose and that of AG/GD are 1/1; (b) Time course of total cell density (OD_{600}); (c) Time course of the percentage of the GD strain in cocultivations. (d)-(e) Initial settings optimization results of salidroside titers for cocultivations of BMT23T2B+BMS24S1 (d) and BMT23T2B+BMS24S2 (e).

4. Discussion

The successful microbial production of a valuable product often depends on the effective channeling of key resources to the desirable metabolic pathways, which holds for both monoculture- and cocultivation-based designs. For cocultivation, additional challenges may arise from the need for maintaining balanced growth of the members

of a synthetic community. In this work, we have investigated, through mathematical modelling and experimentally, a novel ecosystem-based fermentation strategy with combinational QS devices (QS-SLC and QS-MTS) to achieve the desirable goals.

In the IPA case, we have shown through mathematical modelling that the attainable IPA titer depends on the glucose split ratio (r_2/r_1) between IPA production and meeting the cellular needs. As shown by equation 14 and demonstrated by our simulation results, this ratio is determined by the residual glucose concentration and the metabolic switch (MTS) effect (F) of the IPA strain. Within a coculture, both factors are affected by the co-presence of the two strains: while the glucose concentration is clearly a consequence of the balance between the production by the GLU strain and the consumption by the IPA strain, the MTS behavior of the IPA strain is also affected by the competition of the GLU strain within the same growth environment. Our simulation studies have demonstrated that, in a QS-regulated cocultivation system, the time courses of both factors (and hence r_2/r_1) are determined by the chosen QS device and operational settings. Earlier results have shown that the superior IPA cocultivation cases share two important features, namely (1) the rapid release of the BGL enzyme upon the commence of the killing of the GLU strain, resulting in a high glucose concentration, and (2) the rapid MTS response in the IPA strain. As discussed earlier, both features are favorable for improving the glucose split ratio and hence the IPA titer. There is a general trend of a prolonged batch duration (fermentation time) associated with a higher IPA titer (Table S8); this is mainly due to the reduced growth the IPA strain when regulated by MTS.

In the salidroside case, the success critically relies on the balanced growth of the two strains of the cross-feeding coculture. The wide range of testing with four QS-SLC modules (killing-first, antikilling-first, CI-based, and TetR-based modules) and two MTS modules (IPTG-MTS and QS-MTS) showed that to enable the GD strain to sustain the competition from the AG strains, the adoption of regulation (SLC or MTS) devices needed to be combined with a suitable strategy for carbon source supply. In other words, engineered devices for growth and metabolic regulation may be more likely to be successful in challenging applications when utilized within a wider set of

interventions. Furthermore, it appeared that the outcome of such co-cultivation systems could also be significantly affected by the choice of experimental settings such as regulation induction time, carbon source ratio and initial strain ratio, which could be optimized to obtain the best results. In fact, the importance of parameter optimization was also observed in our *in silico* study of IPA production. For example, the initial GLU:IPA strain ratio was shown to be able to affect significantly the trajectory of the system in terms of glucose concentration, the r_2/r_1 ratio, the IPA titer, the cellobiose degradation time, and the fermentation time (Supplementary Fig. S5-S8).

While this work has shown that synthetic genetic circuits, when applied appropriately, could contribute to the success of cocultivation-based production of valuable chemicals, their presence can introduce non-negligible metabolic burdens to their hosts (Goo et al., 2015; Hense and Schuster, 2015). This might have contributed, at least in part, to some of the reduction in productivity following the introduction of engineered devices observed in the salidroside case; exact impacts are yet to be quantified in future work. In our *in silico* study of the IPA case, metabolic burden has not been considered in the mathematical modelling. However, with such possible burdens in mind, we particularly simulated a cocultivation design where only one strain produces the QS signal which is shared by both strains (for lysis and MTS, respectively). This particular case predicted an IPA titer comparable to the best performance that could be achieved by cocultivations without this “economical” measure (Table S8 and S9, Supplementary 1.6). This gives an initial indication of the potential effectiveness of “lighter” designs.

As well as QS-relevant metabolic burden, other complications such as QS crosstalk (Kylilis et al., 2018; Wellington and Greenberg, 2019) and microbial social cheaters (Sandoz et al., 2007; Xavier, 2011), which have not been considered in this work, may also affect the realistic outcome of cocultivation based on combinational QS-based devices and therefore deserve modelling and experimental investigation in the future. Similarly, the modelling study in this work was based on the kinetic parameter values of QS systems calibrated with data available only of pure cultures; it

would be interesting to investigate in the future how these parameter values may deviate in co-cultures.

5. Conclusions

The continued development and applications of QS-based genetic networks are expected to increasingly enable the optimal regulation of synthetic microbial consortia in ecosystem-based fermentation to achieve their goals of synthesis of valuable products. Taking the production of IPA and salidroside as two examples, which each involve both QS-regulated lysis and QS-based metabolic toggle switch (MTS), we have revealed several insights potentially important for future design with respect to the feasibility and optimality of such systems:

- (1) The combined use of QS devices across multiple members offers a new tool to effectively coordinate synthetic microbial consortia for achieving high product titer in cross-feeding cocultivation.
- (2) The performance of QS-regulated cocultivation is shown to be shaped by the QS responses of individual strains which are interconnected through both cross-feeding and growth competition.
- (3) Depending on the specific QS devices used, some configurations could deliver near-optimal performance while some others were shown to be unacceptable, suggesting the importance of choosing the appropriate QS devices in implementing a certain regulation design.
- (4) In addition to the choice of QS devices, other control measures such as the strategies for carbon source supply can be essential for the QS-based control schemes to make a positive contribution, and the optimization of operational settings for a given system configuration can potentially make a significant difference in the attainable performance.

Overall, this work contributes to the revealing of the potential, and the need for optimal design, of combinational QS devices for dynamic control in cross-feeding cocultivations with synthetic microbial consortia.

Code availability

MATLAB Version R2016a were used to develop and solve the mathematical models. The codes are available from the corresponding author upon request.

Acknowledgements

The present study was supported by grants from National Key Research and Development Program of China (No. 2017YFD0201400), the Funds for Creative Research Groups of China (21621004), and National Key Research and Development Program of China (No. 2020YFA0907900).

Competing interests

The authors declare no competing financial interests.

References

- Arora, D., Gupta, P., Jaglan, S., Roullier, C., Grovel, O., Bertrand, S., 2020. Expanding the chemical diversity through microorganisms co-culture: current status and outlook. *Biotechnol. Adv.* 40, 107521. <https://doi.org/10.1016/j.biotechadv.2020.107521>.
- Balagadde, F. K., Song, H., Ozaki, J., Collins, C. H., Barnett, M., Arnold, F. H., Quake, S. R., You, L., 2008. A synthetic *Escherichia coli* predator-prey ecosystem. *Mol. Syst. Biol.* 4, 187-195. <https://doi.org/10.1038/msb.2008.24>.
- Beri, D., York, W. S., Lynd, L. R., Pena, M. J., Herring, C. D., 2020. Development of a thermophilic coculture for corn fiber conversion to ethanol. *Nat. Commun.* 11, 1937. <https://doi.org/10.1038/s41467-020-15704-z>.
- Di, S., Yang, A., 2019. Analysis of productivity and stability of synthetic microbial communities. *J R Soc Interface.* 16, 20180859. <https://doi.org/10.1098/rsif.2018.0859>.
- Din, M. O., Danino, T., Prindle, A., Skalak, M., Selimkhanov, J., Allen, K., Julio, E., Atolia, E., Tsimring, L. S., Bhatia, S. N., 2016. Synchronized cycles of bacterial lysis for in vivo delivery. *Nature.* 536, 81-85. <https://doi.org/10.1038/nature18930>.
- Dinh, C. V., Chen, X. Y., Prather, K. L. J., 2020. Development of a quorum-sensing based circuit for control of coculture population composition in a naringenin production system. *Acs. Synth. Biol.* 9, 9590-9597. <https://doi.org/10.1021/acssynbio.9b00451>.
- Dinh, C. V., Prather, K. L. J., 2019. Development of an autonomous and bifunctional quorum-sensing circuit for metabolic flux control in engineered *Escherichia coli*. *Proc. Natl Acad. Sci. USA.* 116, 25562-25568. <https://doi.org/10.1073/pnas.1911144116>.
- Doong, S. J., Gupta, A., Prather, K. L. J., 2018. Layered dynamic regulation for improving metabolic pathway productivity in *Escherichia coli*. *Proc. Natl Acad. Sci. USA.* 115, 2964-2969. <https://doi.org/10.1073/pnas.1716920115>.
- Du, P., Zhao, H., Zhang, H., Wang, R., Huang, J., Tian, Y., Luo, X., Luo, X., Wang, M., Xiang, Y., Qian, L., Chen, Y., Tao, Y., Lou, C., 2020. De novo design of an intercellular signaling toolbox for multi-channel cell-cell communication and biological computation. *Nat. Commun.* 11, 4226. <https://doi.org/10.1038/s41467-020-17993-w>.

- Elowitz, M. B., Leibler, S., 2000. A synthetic oscillatory network of transcriptional regulators. *Nature*. 403, 335-338. <https://doi.org/10.1038/35002125>.
- Freilich, S., Zarecki, R., Eilam, O., Segal, E. S., Henry, C. S., Kupiec, M., Gophna, U., Sharan, R., Rupp, E., 2011. Competitive and cooperative metabolic interactions in bacterial communities. *Nat. Commun.* 2, 589. <https://doi.org/10.1038/ncomms1597>.
- Goo, E., An, J. H., Kang, Y., Hwang, I., 2015. Control of bacterial metabolism by quorum sensing. *Trends Microbiol.* 23, 567-576. <https://doi.org/10.1016/j.tim.2015.05.007>.
- Gu, F., Jiang, W., Mu, Y. L., Huang, H., Su, T. Y., Luo, Y., Liang, Q. F., Qi, Q. S., 2020. Quorum sensing-based dual-function switch and its application in solving two key metabolic engineering problems. *Acs. Synth. Biol.* 9, 209-217. <https://doi.org/10.1021/acssynbio.9b00290>.
- Gupta, A., Reizman, I. M., Reisch, C. R., Prather, K. L., 2017. Dynamic regulation of metabolic flux in engineered bacteria using a pathway-independent quorum-sensing circuit. *Nat. Biotechnol.* 35, 273-279. <https://doi.org/10.1038/nbt.3796>.
- Hense, B. A., Schuster, M., 2015. Core principles of bacterial autoinducer systems. *Microbiol. Mol. Biol. Rev.* 79, 153-169. <https://doi.org/10.1128/Mmbr.00024-14>.
- Honjo, H., Iwasaki, K., Soma, Y., Tsuruno, K., Hamada, H., Hanai, T., 2019. Synthetic microbial consortium with specific roles designated by genetic circuits for cooperative chemical production. *Metab. Eng.* 55, 268-275. <https://doi.org/10.1016/j.ymben.2019.08.007>.
- Kong, W., Meldgin, D. R., Collins, J. J., Lu, T., 2018. Designing microbial consortia with defined social interactions. *Nat. Chem. Biol.* 14, 821-829. <https://doi.org/10.1038/s41589-018-0091-7>.
- Kylilis, N., Tuza, Z. A., Stan, G. B., Polizzi, K. M., 2018. Tools for engineering coordinated system behaviour in synthetic microbial consortia. *Nat. Commun.* 9, 2677. <https://doi.org/10.1038/s41467-018-05046-2>.
- Liang, D. M., Liu, J. H., Wu, H., Wang, B. B., Zhu, H. J., Qiao, J. J., 2015. Glycosyltransferases: mechanisms and applications in natural product development. *Chem. Soc. Rev.* 44, 8350-8374. <https://doi.org/10.1039/c5cs00600g>.
- Lindemann, S. R., Bernstein, H. C., Song, H. S., Fredrickson, J. K., Fields, M. W., Shou, W., Johnson, D. R., Beliaev, A. S., 2016. Engineering microbial consortia for controllable outputs. *ISME J.* 10, 2077-2084. <https://doi.org/10.1038/ismej.2016.26>.
- Liu, H., Lu, T., 2015. Autonomous production of 1,4-butanediol via a de novo biosynthesis pathway in engineered *Escherichia coli*. *Metab. Eng.* 29, 135-141. <https://doi.org/10.1016/j.ymben.2015.03.009>.
- Liu, J., Li, H., Xiong, H., Xie, X., Chen, N., Zhao, G., Caiyin, Q., Zhu, H., Qiao, J., 2019. Two-stage carbon distribution and cofactor generation for improving l-threonine production of *Escherichia coli*. *Biotechnol. Bioeng.* 116, 110-120. <https://doi.org/10.1002/bit.26844>.
- Liu, X., Li, X. B., Jiang, J., Liu, Z. N., Qiao, B., Li, F. F., Cheng, J. S., Sun, X., Yuan, Y. J., Qiao, J., Zhao, G. R., 2018. Convergent engineering of syntrophic *Escherichia coli* coculture for efficient production of glycosides. *Metab. Eng.* 47, 243-253. <https://doi.org/10.1016/j.ymben.2018.03.016>.
- Miano, A., Liao, M. J., Hasty, J., 2020. Inducible cell-to-cell signaling for tunable dynamics in microbial communities. *Nat. Commun.* 11, 1193. <https://doi.org/10.1038/s41467-020-15056-8>.
- Miller, M. B., Bassler, B. L., 2001. Quorum sensing in bacteria. *Annu. Rev. Microbiol.* 55, 165-199. <https://doi.org/10.1146/annurev.micro.55.1.165>.

- Minty, J. J., Singer, M. E., Scholz, S. A., Bae, C. H., Ahn, J. H., Foster, C. E., Liao, J. C., Lin, X. N., 2013. Design and characterization of synthetic fungal-bacterial consortia for direct production of isobutanol from cellulosic biomass. *Proc. Natl Acad. Sci. USA.* 110, 14592-14597. <https://doi.org/10.1073/pnas.1218447110>.
- Mukherjee, S., Bassler, B. L., 2019. Bacterial quorum sensing in complex and dynamically changing environments. *Nat. Rev. Microbiol.* 17, 371-382. <https://doi.org/10.1038/s41579-019-0186-5>.
- Panossian, A., Wikman, G., Sarris, J., 2010. Rosenroot (*Rhodiola rosea*): traditional use, chemical composition, pharmacology and clinical efficacy. *Phytomedicine.* 17, 481-493. <https://doi.org/10.1016/j.phymed.2010.02.002>.
- Papenfort, K., Bassler, B. L., 2016. Quorum sensing signal-response systems in Gram-negative bacteria. *Nat. Rev. Microbiol.* 14, 576-588. <https://doi.org/10.1038/nrmicro.2016.89>.
- Saini, M., Lin, L. J., Chiang, C. J., Chao, Y. P., 2017. Synthetic consortium of *Escherichia coli* for n-butanol production by fermentation of the glucose-xylose mixture. *J. Agric. Food Chem.* 65, 10040-10047. <https://doi.org/10.1021/acs.jafc.7b04275>.
- Sandoz, K. M., Mitzimberg, S. M., Schuster, M., 2007. Social cheating in *Pseudomonas aeruginosa* quorum sensing. *Proc. Natl Acad. Sci. USA.* 104, 15876-15881. <https://doi.org/10.1073/pnas.0705653104>.
- Scott, S. R., Din, M. O., Bittihn, P., Xiong, L., Tsimring, L. S., Hasty, J., 2017. A stabilized microbial ecosystem of self-limiting bacteria using synthetic quorum-regulated lysis. *Nat. Microbiol.* 2, 17083. <https://doi.org/10.1038/nmicrobiol.2017.83>.
- Scott, S. R., Hasty, J., 2016. Quorum sensing communication modules for microbial consortia. *Acs. Synth. Biol.* 5, 969-977. <https://doi.org/10.1021/acssynbio.5b00286>.
- Soma, Y., Hanai, T., 2015. Self-induced metabolic state switching by a tunable cell density sensor for microbial isopropanol production. *Metab. Eng.* 30, 7-15. <https://doi.org/10.1016/j.ymben.2015.04.005>.
- Song, H., Payne, S., Gray, M., You, L., 2009. Spatiotemporal modulation of biodiversity in a synthetic chemical-mediated ecosystem. *Nat. Chem. Biol.* 5, 929-935. <https://doi.org/10.1038/nchembio.244>.
- Stephens, K., Bentley, W. E., 2020. Synthetic biology for manipulating quorum sensing in microbial consortia. *Trends Microbiol.* 28, 633-643. <https://doi.org/10.1016/j.tim.2020.03.009>.
- Stephens, K., Pozo, M., Tsao, C. Y., Hauk, P., Bentley, W. E., 2019. Bacterial co-culture with cell signaling translator and growth controller modules for autonomously regulated culture composition. *Nat. Commun.* 10, 4129. <https://doi.org/10.1038/s41467-019-12027-6>.
- Tsoi, R., Dai, Z., You, L., 2019. Emerging strategies for engineering microbial communities. *Biotechnol. Adv.* 37, 107372. <https://doi.org/10.1016/j.biotechadv.2019.03.011>.
- Vannini, A., Volpari, C., Gargioli, C., Muraglia, E., Cortese, R., De Francesco, R., Neddermann, P., Di Marco, S., 2002. The crystal structure of the quorum sensing protein TraR bound to its autoinducer and target DNA. *Embo J.* 21, 4393-4401. <https://doi.org/10.1093/emboj/cdf459>.
- Walther, T., François, J. M., 2016. Microbial production of propanol. *Biotechnol. Adv.* 34, 984-996. <https://doi.org/10.1016/j.biotechadv.2016.05.011>.
- Wang, E. X., Liu, Y., Ma, Q., Dong, X. T., Ding, M. Z., Yuan, Y. J., 2019. Synthetic cell-cell communication in a three-species consortium for one-step vitamin C fermentation. *Biotechnol. Lett.* 41, 951-961. <https://doi.org/10.1007/s10529-019-02705-2>.
- Wang, R., Zhao, S., Wang, Z., Koffas, M. A., 2020. Recent advances in modular co-culture engineering

789 for synthesis of natural products. *Curr. Opin. Biotechnol.* 62, 65-71.
790 <https://doi.org/10.1016/j.copbio.2019.09.004>.

791 Wellington, S., Greenberg, E. P., 2019. Quorum sensing signal selectivity and the potential for
792 interspecies cross talk. *mBio.* 10, e00146-19. <https://doi.org/10.1128/mBio.00146-19>.

793 Wu, J., Bao, M., Duan, X., Zhou, P., Chen, C., Gao, J., Cheng, S., Zhuang, Q., Zhao, Z., 2020a.
794 Developing a pathway-independent and full-autonomous global resource allocation strategy to
795 dynamically switching phenotypic states. *Nat. Commun.* 11, 5521.
796 <https://doi.org/10.1038/s41467-020-19432-2>.

797 Wu, S., Liu, J., Liu, C., Yang, A., Qiao, J., 2020b. Quorum sensing for population-level control of
798 bacteria and potential therapeutic applications. *Cell. Mol. Life Sci.* 77, 1319-1343.
799 <https://doi.org/10.1007/s00018-019-03326-8>.

800 Wu, S., Xu, C., Liu, J., Liu, C., Qiao, J., 2021. Vertical and horizontal quorum-sensing-based
801 multicellular communications. *Trends Microbiol.* <https://doi.org/10.1016/j.tim.2021.04.006>.

802 Xavier, J. B., 2011. Social interaction in synthetic and natural microbial communities. *Mol. Syst. Biol.*
803 7, 483. <https://doi.org/10.1038/msb.2011.16>.

804 Yang, D., Park, S. Y., Park, Y. S., Eun, H., Lee, S. Y., 2020. Metabolic Engineering of *Escherichia coli*
805 for Natural Product Biosynthesis. *Trends Biotechnol.* 38, 745-765.
806 <https://doi.org/10.1016/j.tibtech.2019.11.007>.

807 Yao, Y. F., Wang, C. S., Qiao, J., Zhao, G. R., 2013. Metabolic engineering of *Escherichia coli* for
808 production of salvianic acid A via an artificial biosynthetic pathway. *Metab. Eng.* 19, 79-87.
809 <https://doi.org/10.1016/j.ymben.2013.06.001>.

810 You, L., Cox, R. S., 3rd, Weiss, R., Arnold, F. H., 2004. Programmed population control by cell-cell
811 communication and regulated killing. *Nature.* 428, 868-871.
812 <https://doi.org/10.1038/nature02491>.

813 Zhang, H., Pereira, B., Li, Z., Stephanopoulos, G., 2015. Engineering *Escherichia coli* coculture
814 systems for the production of biochemical products. *Proc. Natl Acad. Sci. USA.* 112, 8266-
815 8271. <https://doi.org/10.1073/pnas.1506781112>.

816 Zhang, H., Wang, X., 2016. Modular co-culture engineering, a new approach for metabolic
817 engineering. *Metab. Eng.* 37, 114-121. <https://doi.org/10.1016/j.ymben.2016.05.007>.

818 Zhou, K., Qiao, K., Edgar, S., Stephanopoulos, G., 2015. Distributing a metabolic pathway among a
819 microbial consortium enhances production of natural products. *Nat. Biotechnol.* 33, 377-383.
820 <https://doi.org/10.1038/nbt.3095>.